small structures
www.small-structures.com

Chiral Display of Pyrenes on a Peptoid Backbone: Conformational Homogeneity of Peptoid Controls Excimer Chirality

Jinyoung Oh, Yongmoon Lee, Gahee Noh, Dongcheol Park, Hohjai Lee, Junseong Lee, Changsoon Kim,* and Jiwon Seo**

Controlling chromophore chirality in three-dimensional space is crucial for understanding the structure–chiroptical relationship. Such control enables the prediction of ideal materials for use in chiral photonic applications. In this study, optically active multipyrene systems are synthesized on peptoids. Pyrene-based chiral submonomers, (*S*)- and (*R*)-1-pyrenylethylamine (s1pye and r1pye), are successfully incorporated into peptoids as the respective (*S*)- and (*R*)-*N*-(1-pyrenylethyl)glycine (*Ns*1pye and *Nr*1pye) units. NMR spectroscopy revealed length- and *N*-acetylation-dependent conformational homogeneity enhancement in solution, stabilizing *cis*-amides in *Ns*1pye-containing peptoids. The X-ray crystal structure of *Ns*1pye tetramer displayed a polyproline type-I (PPI)-like helix. All of the pyrene-related absorptions are circular dichroism (CD) active, and the CD signal related to the long-axis-polarized transition increased with helical stabilization. Intramolecular excimer generation yielded significant circularly polarized luminescence (CPL) in the excimer emission region. Early-stage peptoids emitted left-handed CPL, but upon acquiring a PPI-like helix character, CPL handedness became inverted. The CPL dissymmetry factor (g_{lum}) was comparable or superior (10^{-2}) to that of chiral organic dyes (10^{-5}–10^{-2}). This new class of helical pyrene-containing peptoids provides a CPL-active intramolecular excimer, modulating optical activity through peptoid secondary structure homogeneity.

1. Introduction

Peptoids are a class of non-natural heteropolymers composed of *N*-substituted glycine backbones.[1] In contrast to peptides, the side chains of peptoids are connected to the amide nitrogen atoms. Therefore, peptoids lack the hydrogen bonds between backbone amides that are responsible for the formation of secondary structures in peptides (**Figure 1**A). Instead, the incorporation of chiral side chains results in transfer of the chirality to the peptoid backbone,[2–4] and steric and electronic interactions between the side chains and the backbone amides induce a defined chiral fold.[5–9] In particular, a helical conformation can be stabilized by introducing various bulky chiral side chains, including aromatic[8,9] and aliphatic ones.[6,10] Peptoid helices display a propensity to adopt a polyproline type-I (PPI) helix, with a 6 Å pitch distance and three residues per turn.[3] Following the discovery of these helices, peptoids have been shown to mimic diverse natural secondary structures, including loops[11] and turns.[12] The defined structure of peptoids can serve as a basis for their rational design. Studies of peptoid systems bearing membrane-active amphiphiles,[13] metal-binding ligands,[14,15] enantioselective catalysts,[16] energy transfer systems,[17] and electron transfer systems[18] have revealed their structure-driven properties and functions.

A broad conformational space has been sampled using various peptoid sequences, mostly for the formation of stable and conformationally homogeneous helices. Initial studies focused on peptoids containing (*S*)-*N*-(1-phenylethyl)glycine (*N*spe) residues, which provide sufficient bulkiness to induce a *cis*-amide helix. The *N*spe residue has been widely used and has become the gold standard for generating peptoid helices. However, *N*spe

J. Oh, D. Park, H. Lee, J. Seo
Department of Chemistry
Gwangju Institute of Science and Technology (GIST)
123 Cheomdangwagi-ro, Buk-gu, Gwangju 61005, Republic of Korea
E-mail: jseo@gist.ac.kr

Y. Lee, C. Kim
Graduate School of Convergence Science and Technology
Seoul National University
1 Gwanak-ro, Gwanak-gu, Seoul 08826, Republic of Korea
E-mail: changsoon@snu.ac.kr

G. Noh, J. Lee
Department of Chemistry
Chonnam National University
77, Yongbong-ro, Buk-gu, Gwangju 61186, Republic of Korea
E-mail: leespy@chonnam.ac.kr

The ORCID identification number(s) for the author(s) of this article can be found under https://doi.org/10.1002/sstr.202300396.

DOI: 10.1002/sstr.202300396

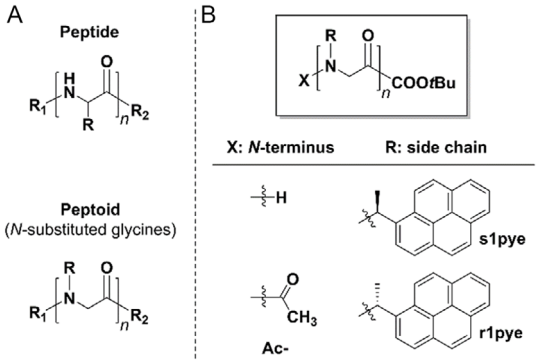

Figure 1. A) Chemical structures of peptides and peptoids. B) Peptoids discussed in this study.

residues often stabilize both *cis*- and *trans*-amides when other noncovalent interactions are involved (e.g., to form a threaded-loop structure for a nonameric *N*spe peptoid).[11] Therefore, peptoid monomers with greater propensity to stabilize the *cis*-amides are desirable for maintaining homogeneous secondary structures under a variety of conditions. Blackwell and co-workers previously surveyed the sequence–structure relationships using a diverse array of peptoid monomers, which revealed (*S*)-*N*-(1-naphthylethyl)glycine (*N*s1npe) residues to be particularly effective in promoting formation of the *cis*-rotamer.[19] The peptoid helices were primarily formed because of the substantial steric hindrance between the bulky naphthalene-containing side chains, which mediated a significant *cis*-amide-inducing effect with PPI-like structural features.[9] First used in peptoids by Blackwell's group, naphthalene has often been exploited to induce helical structures,[20] as a fluorescence emitter,[21] and to generate excimers.[22] However, understanding the photophysical properties of peptoids based on their structure poses a challenge owing to the lack of clear relationships between the secondary structures of peptoids and their spectral characteristics.

Circular dichroism (CD), for example, is a valuable method for determining the secondary structures of peptides, peptoids, and proteins.[2,11] Exciton-coupled signals at approximately 192 nm and 202 nm and a negative transition signal at approximately 220 nm are characteristic signatures of *N*spe-based helical peptoids. However, the CD spectra of naphthalene-containing peptoids are difficult to interpret on an individual component basis because the UV absorption of naphthalene overlaps with that of the backbone amide groups. It is envisioned that the replacement of naphthalene with pyrene would enhance the understanding of how the secondary structure affects the CD profile in the presence of the CD-active luminophore. Furthermore, the extended conjugation system allows for longer-wavelength emission, opening the way to the development of peptoids as fluorescence emission controllers.

It is hypothesized that if the chiral environment offered by the helical peptoid could allow chiral absorption by the luminophore, the chiral emission would also be affected by the environment. One important phenomenon for understanding chiral emission properties is the circularly polarized luminescence (CPL), which refers to a difference in the emission intensity between left- and right-handed circularly polarized light. The discovery of efficient CPL emitters has enabled improvements in various technical applications, including biological sensing[23] and imaging,[24] data encryption,[25] and enantioselective synthesis.[26,27] CPL from chiral luminophores provides a facile method for producing circularly polarized light, and various organic materials have recently been reported to display CPL activity after incorporating chirality into luminescent molecules.

However, the luminescence dissymmetry factor (g_{lum}), which reflects the degree of asymmetry between left-handed CPL (LCPL) and right-handed CPL (RCPL), is generally low for organic molecules (10^{-5}–10^{-2}).[28–31] In an effort to overcome this limitation, co-assembled structures of organic molecules have been investigated, leading to higher dissymmetry factors.[32,33] The resulting exciton coupling can improve the CPL dissymmetry in highly ordered molecularly stacked systems. However, the construction of such systems requires a large number of molecules, and their arrangement must be directed toward the enhancement of dissymmetry, which is difficult to modulate and predict. Therefore, a powerful CPL amplification strategy could be the construction of a CPL emission system based on intramolecular interactions between luminophores that are controllable via the secondary structure of an appropriate scaffold molecule. In this regard, peptoid helices offer the potential to enhance the dissymmetry by tailoring the building blocks to obtain defined secondary structures in which the distance and angle of the chromophores can be controlled.

In this work, pyrene-containing helix-inducing peptoid submonomers were synthesized and the pyrene moieties were helically displayed on peptoid backbones with varying degrees of structural homogeneity. A comprehensive structural study was conducted using NMR spectroscopy and X-ray crystallography. Photophysical characterization was performed by absorption and CD analysis for the ground state and by fluorescence and CPL analysis for the excited state. This work provides the first example of CPL-generating peptoids reported to date, and an unprecedented chiral inversion with increasing structural homogeneity is demonstrated. The results suggest that chromophore-containing peptoids can serve as promising optically active scaffolds for understanding the relationship between structure and optical properties.

2. Results and Discussion

2.1. Synthesis of Peptoid Oligomers

Pyrene-containing *Nα* chiral submonomers ((*S*)-1-pyrenylethylamine, s1pye; (*R*)-1-pyrenylethylamine, r1pye) were synthesized by a previously reported method[34] using Ellman's chiral auxiliaries (*tert*-butanesulfinamides) (Scheme S1, Supporting Information). Peptoids can be obtained via solid-phase[35] or solution-phase[9,10,36] submonomer synthesis procedures. In the case of the (*S*)-*N*-(1-pyrenylethyl)glycine (*N*s1pye) homooligomers, a conventional solid-phase peptoid synthesis approach, using bromoacetic acid/DIC coupling, did not allow for bromoacetylation following the second residue, necessitating the use of previously reported solution-phase synthetic methods.[9,10] For the *C*-terminal end group, the *tert*-butyl ester was selected to avoid

Table 1. Sequences of **1**–**7**, **1′**–**7′**, $\mathbf{2}_{R}$, and $\mathbf{2'}_{R}$.

	Monomer sequence		Monomer sequence
1	H-*N*s1pye-COO*t*Bu	**1′**	Ac-*N*s1pye-COO*t*Bu
2	H-(*N*s1pye)$_2$-COO*t*Bu	**2′**	Ac-(*N*s1pye)$_2$-COO*t*Bu
3	H-(*N*s1pye)$_3$-COO*t*Bu	**3′**	Ac-(*N*s1pye)$_3$-COO*t*Bu
4	H-(*N*s1pye)$_4$-COO*t*Bu	**4′**	Ac-(*N*s1pye)$_4$-COO*t*Bu
5	H-(*N*s1pye)$_5$-COO*t*Bu	**5′**	Ac-(*N*s1pye)$_5$-COO*t*Bu
6	H-(*N*s1pye)$_6$-COO*t*Bu	**6′**	Ac-(*N*s1pye)$_6$-COO*t*Bu
7	H-(*N*s1pye)$_7$-COO*t*Bu	**7′**	Ac-(*N*s1pye)$_7$-COO*t*Bu
$\mathbf{2}_{R}$	H-(*N*r1pye)$_2$-COO*t*Bu	$\mathbf{2'}_{R}$	Ac-(*N*r1pye)$_2$-COO*t*Bu

intramolecular hydrogen bonding, which is known to have an impact on the peptoid secondary structure.[11] In addition, previous studies have demonstrated that *C*-terminal *tert*-butyl esters possess the ability to promote crystallization.[9,10,20] Peptoids were synthesized with and without an *N*-acetyl group to investigate the influence of *N*-terminal capping on the conformational homogeneity of the secondary structure (Figure 1B).[37] The synthesis began with a substitution reaction between *tert*-butyl bromoacetate and s1pye to yield monomer **1**. The peptoids were then elongated by repeating a reaction cycle comprising acylation with bromoacetyl bromide followed by displacement with s1pye. After each displacement step, *N*-terminal acetylation was conducted using acetic anhydride to afford peptoids **1′**–**7′** (Figure S2, Supporting Information, **Table 1**).

2.2. NMR Analysis

Conformational homogeneity of peptoids were evaluated by NMR spectroscopy. $K_{cis/trans}$ is an indicative parameter to quantify the homogeneity of PPI-like peptoid helices, which are composed of backbone cis-amides (**Figure 2**). Following previously described methods,[11,38] the peaks corresponding to *cis*- and *trans*-amide rotamers were identified via 2D ^{1}H–^{1}H NOESY and 2D ^{1}H–^{13}C HSQC experiments. Then, the integrals of the rotamer-related peaks in the 1D ^{1}H NMR and 2D ^{1}H–^{1}H COSY spectra were used to calculate the $K_{cis/trans}$ values (**Table 2**). The *N*s1pye homooligomer successfully stabilized the *cis*-rotamer upon chain elongation. The overall backbone amide $K_{cis/trans}$ value of **2′** in acetonitrile was 11.4, which is the highest value reported for any peptoid dimer to date. Trimeric peptoid **3′** exhibited a $K_{cis/trans}$ value of greater than 19, which surpasses that previously reported for the naphthyl-based peptoid Ac-(*N*s1npe)$_3$-COO*t*Bu ($K_{cis/trans} = 16.0$).[9] The bulky pyrene-containing side chain led to a general trend of increasing $K_{cis/trans}$ values with increasing peptoid length. Compared with naphthalene, pyrene possesses a lower LUMO, which should promote the noncovalent interaction between the nonbonding orbital of the backbone carbonyl group and the π* orbital of pyrene (nπ*$_{Ar}$ effect).[7] Compared with **1′**–**5′**, peptoids **1**–**5** displayed significantly decreased $K_{cis/trans}$ values. Unlike peptides, the side chains of peptoids are attached to the nitrogen atoms; thus, the first residue from the *N*-terminus is susceptible to nitrogen inversion, resulting in conformational

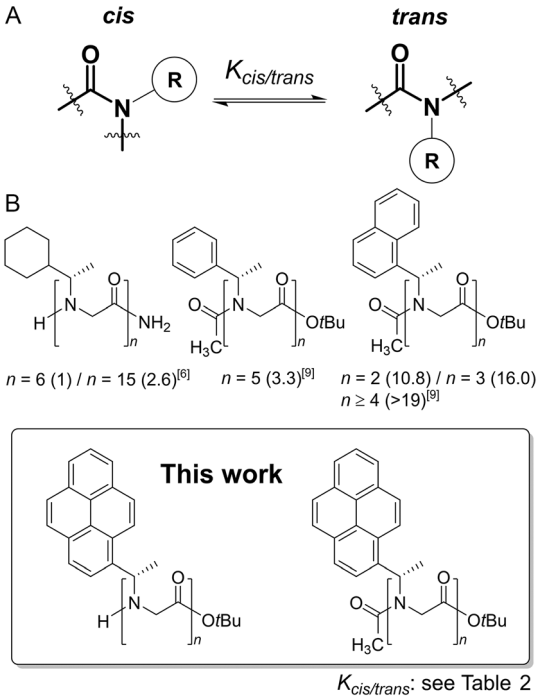

Figure 2. A) Backbone amide cis–trans isomerism. B) $K_{cis/trans}$ values of various peptoids determined by NMR.

Table 2. Overall $K_{cis/trans}$ values as determined by integration of the ^{1}H NMR or ^{1}H–^{1}H COSY spectra in CD_3CN.

	Monomer sequence		Monomer sequence
1	N.A.	**1′**	4.1[b]
2	0.7[a]	**2′**	11.4[b]
3	1.9[a]	**3′**	>19[b]
4	2.2[a]	**4′**	>19[a]
5	5.8[a]	**5′**	>19[a]

[a]Determined by integration of 2D ^{1}H–^{1}H COSY spectra. [b]Determined by integration of 1D ^{1}H NMR spectra.

heterogeneity of the overall structure. The *N*-terminal acetylation in **1′**–**5′** clearly suppressed the *trans*-rotamer population at the *N*-terminus to afford enhanced conformational homogeneity. The $K_{cis/trans}$ values of peptoids **6**, **6′**, **7**, and **7′** could not be measured on account of their limited solubility in acetonitrile.

2.3. X-ray Crystallography

Peptoids **1**, **2**, and **1′**–**4′** were crystallized (the conditions are given in Table S3, Supporting Information) and their solid-state structures were determined by single-crystal X-ray crystallography (**Figure 3**).[39] The development of the peptoid helix was visualized using the crystal structures of peptoids **1′**–**4′** (Figure 3A). Peptoid **4′** exhibited a pitch of ≈6 Å and approximately three residues per turn, in accordance with previous studies.[9,10] The torsional angles of peptoids **1**, **2**, and **1′**–**4′** are listed in

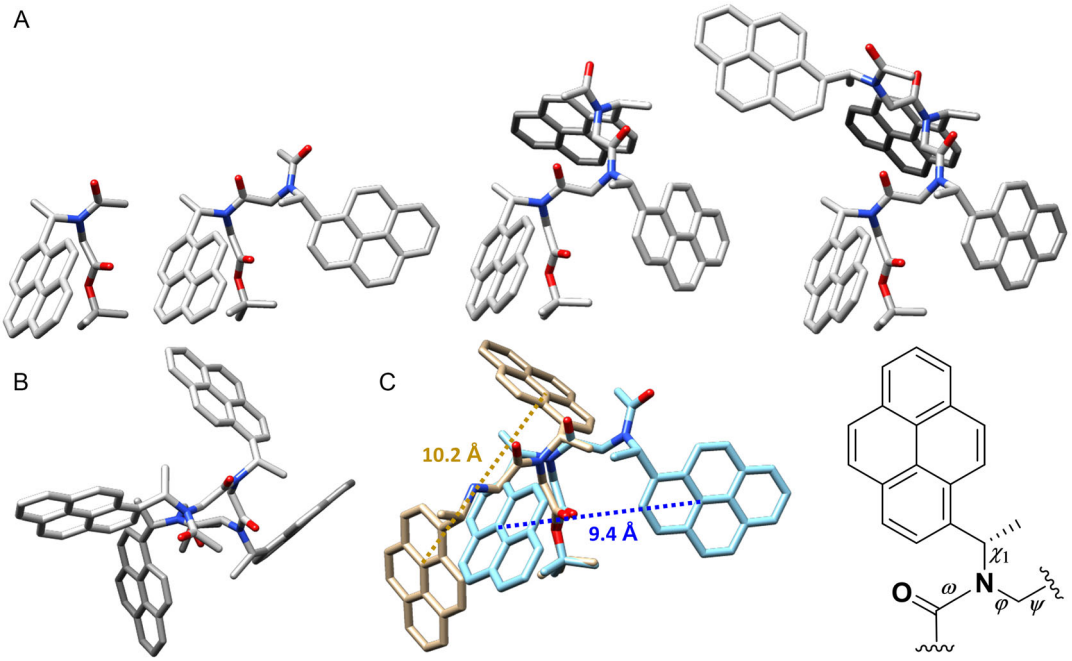

Figure 3. A) Solid-state structures of peptoids **1′**–**4′** as determined by X-ray crystallography. B) View parallel to the helical axis from the *N*-terminus of peptoid **4′**. C) Overlay of the molecular structures of peptoids **2** (beige) and **2′** (cyan).

Table 3. Torsion angles of peptoids **1**, **2**, and **1′**–**4′** as determined by X-ray crystallography.

	Residue	ω	Φ	ψ	χ_1
1	1	–	–	169.1	–
2	1	–	–	–174.6	–
	2	–4.6	–72.6	173.1	–136.9
1′	1	1.5	85.7	155.2	–135.0
2′	1	–10.4	–77.2	–166.4	–123.0
	2	–6.7	87.3	160.8	–132.7
3′	1	–4.5	–77.4	–176.6	–132.9
	2	–15.5	–69.2	–177.7	–135.1
	3	–0.1	86.3	153.9	–126.4
4′	1	–1.3	–86.0	–173.2	–79.4
	2	–12.6	–73.4	–176.2	–130.3
	3	–12.8	–72.4	–173.8	–130.4
	4	–5.1	89.3	150.7	–126.6

Table 3. Deviation of the amide bond planarity was observed, as demonstrated by the ω angles ranging from −15.5° to 1.5°. Nonplanar amide bonds have been reported previously for constrained cyclic peptoids[12] and helical peptoids bearing bulky side chains[9,10]; the deviation observed for the pyrene-containing side chain s1pye may be attributable to its similarity to the latter case. Notably, the $n\pi^*_{Ar}$ interaction was not observed in the solid state. Unlike the solution state, a condensed solid-state environment may prioritize the packing of molecules over their intramolecular interactions. For example, intermolecular π–π stacking between the pyrene side chains was observed for peptoids **1** and **4′** (Figure S3, Supporting Information). Similar structural features were observed for the previously reported naphthyl-based peptoids.[9] The structural difference between the solid and solution states was observed for the dimeric peptoids. Specifically, peptoid **2** exhibited a *cis*-amide structure (Figure 3C), which was not a major conformation in solution ($K_{cis/trans} = 0.7$ in acetonitrile). Compared with peptoid **2′**, the structure of peptoid **2** featured a longer distance between the two pyrene moieties, demonstrating the flexibility of the peptoid without *N*-acetyl capping.

2.4. CD Spectroscopy

The CD spectra of *N*spe-based helical peptoids have been extensively investigated.[5,40] The orbital interactions between the backbone carbonyl and side chain phenyl groups result in $\pi\rightarrow\pi^*_{Ar}$ (≈192 nm and 202 nm) and $n\rightarrow\pi^*_{Ar}$ (≈220 nm) transitions, providing a CD signature that is similar to that of PPI-type helical peptides.[2,5] Subsequently, helical peptoids containing naphthyl-[9] and alkyl-based side chains[6,10] were characterized by NMR spectroscopy and X-Ray crystallography; however, the unusual CD signature of these folded peptoids has yet to be rationalized.[6,9,10] Herein, an attempt has been made to explain the nature of each peak observed in the CD spectra of the pyrene-containing peptoids. First, the absorption spectra of the pyrene-containing peptoid series are recorded to investigate the electronic and vibrational modes of the pyrene moieties (Figure S5, Supporting Information). The pyrene absorption spectra displayed the distinctive electronic states of ^1L_a (S_2–S_0, $\lambda_{max} = 344$ nm), ^1B_b (S_3–S_0, $\lambda_{max} = 277$ nm), and ^1B_a (S_4–S_0, $\lambda_{max} = 242$ nm), but not the symmetrically forbidden state ^1L_b

(S_1–S_0).[41] Because the entire set of vibronic states was maintained in the *N*s1pye oligomers, the neighboring 1-ethylamine substituent and amide groups had minimal effect on the vibronics of the pyrene moieties. For the pyrene moieties of the *N*s1pye oligomers, every absorption (^1L_a, ^1B_b, and ^1B_a) is CD active, and multiple Cotton effects were observed (**Figure 4**A–C). The through-space coupling of adjacent chromophores in a chiral environment generates exciton-coupled circular dichroism (ECCD), which can be experimentally identified by a bisignate CD couplet.[42,43] Except for the **1**, **1′**, **2**, **2′**, and **3**, the negative Cotton effect for the ECCD signals of the ^1L_a and ^1B_a states gradually increased for both sets of peptoids in a length-dependent manner (Figure 4B,C). These results indicate that the interaction between the long-axis-polarized transition dipoles (^1L_a and ^1B_a) became stronger as the peptoid length increased from a trimer to a heptamer. The ECCD intensity is proportional to the cross product of the two transition dipoles (i.e., $|\boldsymbol{\mu}_1 \times \boldsymbol{\mu}_2|$) and inversely proportional to the interchromophore distance.[42,43] Therefore, it is assumed that as the peptoid elongated from a trimer to a heptamer, the transition dipoles (^1L_a and ^1B_a) became located near each other in space and oriented away from a parallel (or anti-parallel) alignment. In contrast, the ECCD signal of the short-axis-polarized transition dipole ^1B_b tended to decrease. This suggests that peptoid elongation caused the ^1B_b transition dipoles to align parallel to one another, resulting in a decrease in $|\boldsymbol{\mu}_1 \times \boldsymbol{\mu}_2|$. The negative Cotton effect in ECCD indicates a counterclockwise arrangement (i.e., right-handed helical sense) of the pyrene moieties in the peptoid helix, which is in accordance with the X-ray crystal structures of **3′** and **4′** (Figure 3). The overall similarity of the CD signatures between peptoids **3**–**7** and **3′**–**7′** provides convincing evidence that the *N*s1pye oligomers folded into the right-handed helical structure irrespective of the presence or absence of *N*-acetylation. Similar to the results obtained by NMR spectroscopy (Table 2), a more homogeneous conformation was demonstrated for *N*-acetylated peptoids based on the stronger CD intensities observed for peptoids **3′**–**7′**. The *N*-terminal acetylation holds promise for diminishing the average intramolecular distance between pyrenes, subsequently resulting in an improvement in ECCD signal. For example, heptameric **7** and tetrameric **4′** exhibited similar CD intensities (Figure 4D). Notably, peptoid **2** afforded a distinctive CD profile with an inverse signal for the ^1B_a state, indicating that the optical environment of the pyrene moieties in peptoid **2** was different from those in the longer peptoids. The enantiomers of **2** and **2′** (i.e., $\mathbf{2}_R$ and $\mathbf{2'}_R$) were synthesized using the r1pye submonomer and found to display CD spectra that were clear mirror images (Figure 4E)

2.5. Fluorescence Measurements and Excimer Characterization

The excimer emission represents the electronic perturbation induced by interactions between luminophores in the excited state. Fluorescence spectra were collected at an excitation wavelength of 355 nm (**Figure 5**). The excimer emission of peptoids **2**–**7** was observed at an emission wavelength (λ_{em}) of 458–466 nm, while the *N*-acetylated peptoids **5′**–**7′** exhibited excimer emission at 444 nm. Peptoid **2** displayed a unique behavior with early-stage excimer generation (Figure 5A). In the solution state, the heterogeneity of this peptoid brings the two pyrenes into close proximity, facilitating the generation of the excimer state. As shown by both CD and fluorescence spectra, the pyrene arrangement in peptoid **2** did not correlate with

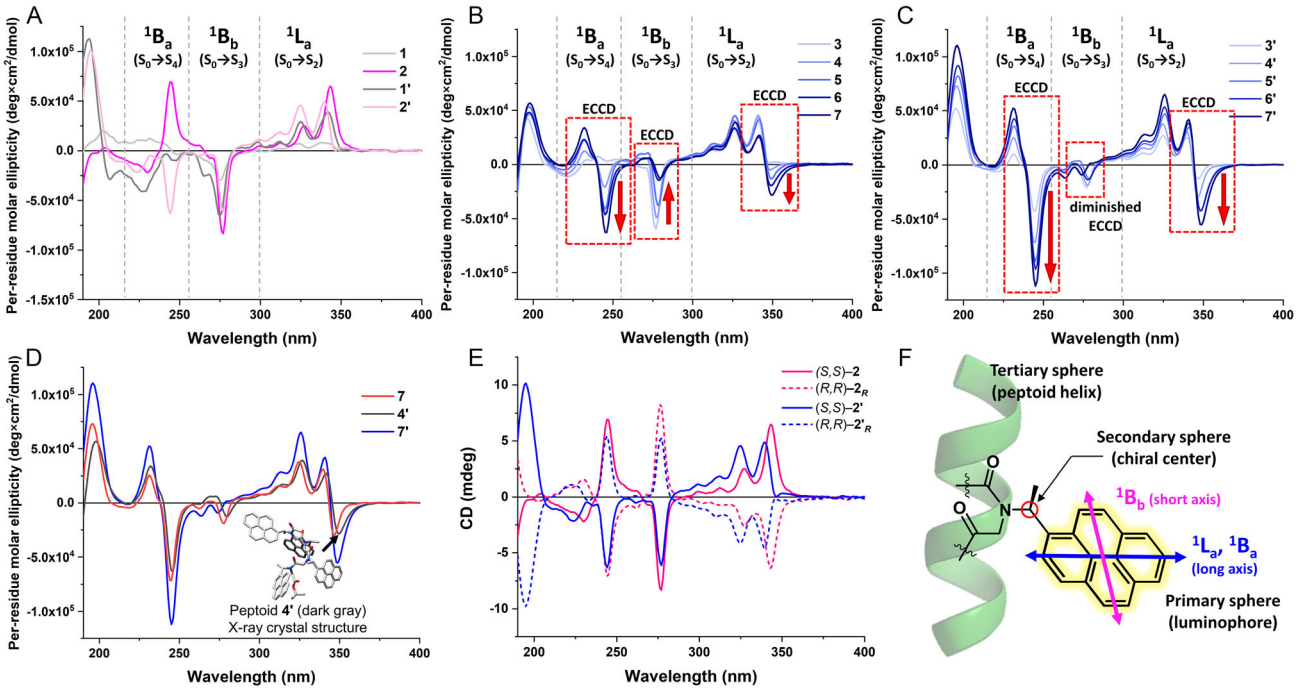

Figure 4. CD spectra of *N*s1pye homooligomers A) **1**, **2**, **1′**, and **2′**, B) **3**–**7**, C) **3′**–**7′**, D) **4′**, **7**, and **7′**, and E) **2** and **2′** alongside their enantiomers ($\mathbf{2}_R$ and $\mathbf{2'}_R$) at 50 μM in acetonitrile. F) Schematic geometry representation of CD generation by the peptoids.

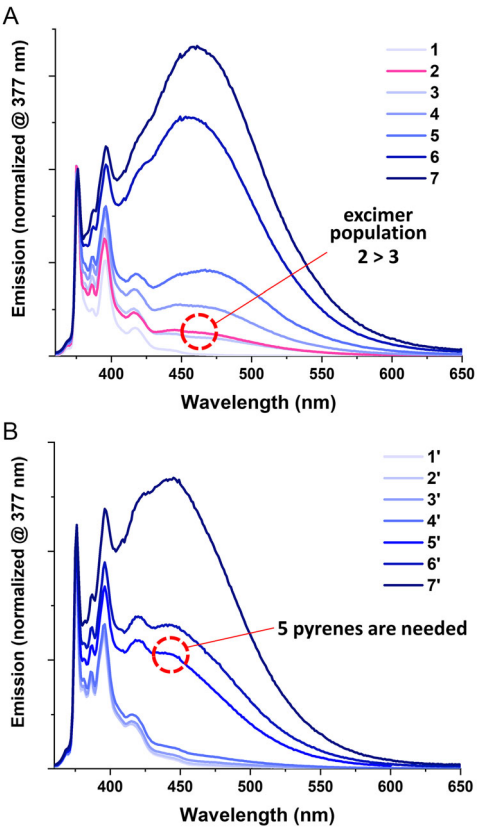

Figure 5. Fluorescence spectra of *N*s1pye homooligomers A) **1**–**7** and B) **1′**–**7′** at 50 μM in degassed acetonitrile ($\lambda_{ex} = 355$ nm).

that of the longer peptoids. After *N*-acetylation, excimer formation was suppressed in peptoids **2′**–**4′**, which was likely attributable to a reduction in the conformational flexibility necessary to generate the excimer state between the pyrene moieties (Figure 5B). A distinct excimer peak appeared for peptoid **5′** and longer oligomers.

2.6. CPL Measurement and Chirality Inversion

CPL measurements were performed to examine the excimer chirality of the pyrene-containing peptoids. Peptoids **2**–**7** and **2′**–**7′** were found to exhibit CPL activity with a high dissymmetry factor ($g_{lum} = 10^{-2}$, **Table 4** and **Figure 6**). The absence of dissymmetry

Table 4. Dissymmetry factors (g_{lum}) of *N*s1pye homooligomers **1**–**7** and **1′**–**7′**.

	g_{lum} [$\times 10^{-2}$]		g_{lum} [$\times 10^{-2}$]
1	N.A.	**1′**	N.A.
2	1.75	**2′**	0.51
3	0.79	**3′**	–0.59
4	0.79	**4′**	–1.06
5	–0.26/0.38	**5′**	–1.29
6	–0.78	**6′**	–1.28
7	–0.74	**7′**	–1.23

(or CPL activity) for local emission (<400 nm) indicates that the formation of the chiral excimers is crucial for generating CPL emission in the *N*s1pye oligomer system. For this reason, monomeric peptoids **1** and **1′** did not display CPL activity. The generation of LCPL and RCPL was found to be influenced by the structural homogeneity of the ground state. As the peptoid chain became longer and after *N*-acetylation, the dissymmetry tended to enhance RCPL (Figure 6). The largest positive g_{lum} value was observed for the dimeric peptoid **2** ($g_{lum} = 1.75 \times 10^{-2}$), while the largest negative g_{lum} values were found for the conformationally homogeneous peptoids **5′**–**7′** ($g_{lum} = -1.3 \times 10^{-2}$). The opposite sign of g_{lum} for peptoid **2**, compared with the longer peptoids, indicates the opposite chirality of the pyrene excimer. The unique chiroptical properties of peptoid **2** were also observed in the CD spectra (Figure 4A). The strong intensities of the ECCD peaks for peptoid **2**, along with its distinct spectral signature, particularly the positive Cotton effect for the long-axis transitions (^1L_a and ^1B_a), align well with the CPL results. Peptoids **4** and **5** exhibited wavelength-dependent CPL sign inversion. RCPL and LCPL were recorded at shorter and longer wavelengths, respectively. This implies that these peptoids with moderate conformational homogeneity form multiple excimer conformations in the excited state, each with distinct optical activity. Peptoids **2**–**7** and **2′**–**7′** exhibited saturation of luminescence (g_{lum}) at specific lengths (i.e., the hexamer and pentamer, respectively). Besides the dissymmetry factor, a high excimer quantum yield is another prerequisite for an efficient CPL emitter. In the trimeric and longer peptoids (**3**–**7** and **3′**–**7′**), a tendency of increasing quantum yield with greater peptoid length was observed (Table S5, Supporting Information). Therefore, **7′** can be considered an efficient CPL emitter compared with the other pyrene-containing peptoid helices. The intricate structural features of flexible and multichromophore-containing system make it challenging to undertake a detailed structure-based CPL rationallization. However, these results suggest that a chromophore display strategy based on peptoid helices is a versatile method for generating excimer CPL.

3. Conclusion

A series of optically active peptoids, displaying multiple pyrene moieties, were synthesized. Characterization of the structures and photophysical properties of the prepared 1-pyrene-containing peptoids (i.e., *N*s1pye oligomers) revealed valuable insights into the relationship between conformational homogeneity and optical activity. The helical propensity of the *N*s1pye oligomers is examined using NMR spectroscopy and observed stabilization of the *cis*-amide backbone upon sequence elongation and *N*-terminal acetylation. Peptoid **3′** started to exhibit significant *cis*-amide stabilization ($K_{cis/trans} > 19$ in acetonitrile), affording one of the most conformationally stable trimeric peptoids reported to date. The X-Ray crystal structure of the *N*-acetylated tetramer **4′** demonstrated the progression of a right-handed PPI-like helix, as confirmed by backbone torsion angles that were similar to those of previously reported PPI-like peptoid helices.[9] This well-defined structure served as the foundation for our interpretation of the CD spectra, providing a practical solution for situations where multiple transitions from the incorporated

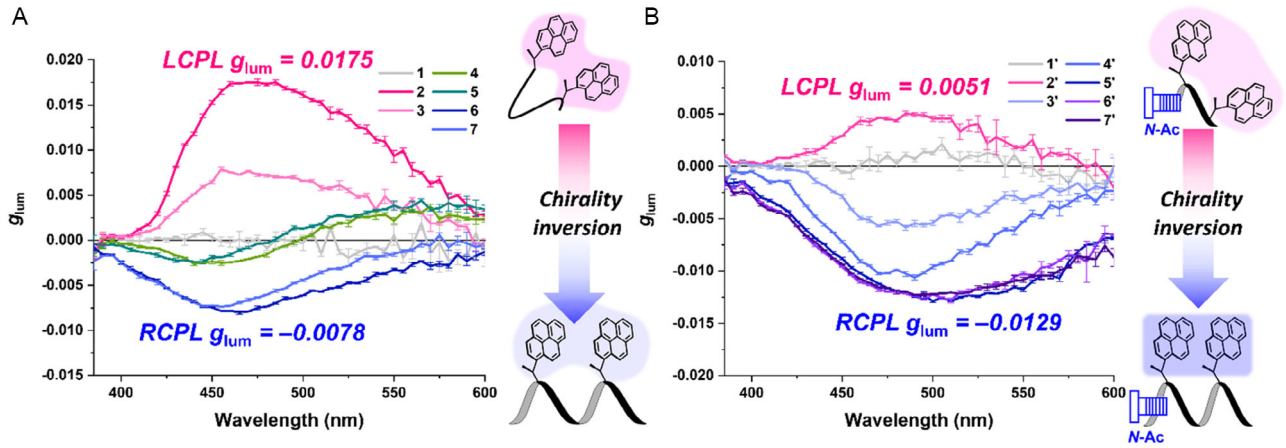

Figure 6. CPL spectra of *N*s1pye homooligomers A) **1**–**7** and B) **1′**–**7′** at 50 μM in acetonitrile.

chromophores are CD active. In the case of pyrene, the perpendicular property between the long- and short-axis-polarized transitions induced the opposite tendency of change in the ECCD intensity in a length-dependent manner.

The incorporation of multiple pyrene units in the peptoids resulted in not only chiral absorption but also the formation of chiral pyrene excimer fluorescence. Notably, the non-acetylated peptoid dimer **2** exhibited an intramolecular excimer generating LCPL with a significant dissymmetry factor ($g_{lum} = 1.75 \times 10^{-2}$). *N*-Acetylation and elongation promoted the formation of a more homogeneous secondary structure, resulting in a more negative CPL (RCPL), which became saturated at the pentamer length (**5′**). Our results with the *N*s1pye homooligomers indicated that flexible short peptoids tend to emit LCPL and long peptoids with structural homogeneity tend to emit RCPL. On the basis of the proposed structure–photophysical property relationship, our peptoid series may broaden the understanding of multichromophoric chiral systems and expand the potential applications of biomimetic scaffolds in the fields of imaging and sensing.

Supporting Information

Supporting Information is available from the Wiley Online Library or from the author.

Acknowledgements

J.O. and Y.L. contributed equally to this work. This work was financially supported by the National Research Foundation of Korea (NRF-2021R1A2C2014421 and RS-2023-00217317 to J.S. and NRF-2021R1A4A1032515 to C.K.) and by the Creative Materials Discovery Program (NRF-2018M3D1A1052659 to J.S.), which is funded by the National Research Foundation (NRF) under the Ministry of Science and ICT. C.K. is grateful for the financial support from the Samsung Research Funding Center of Samsung Electronics (SRFC-MA1602-51). J.S. is grateful to the Korean Basic Science Institute (KBSI) in Ochang for instrumentation support (900 MHz NMR measurements). [Correction added on 09 December 2023, after first online publication: Affiliation corrected]

Conflict of Interest

The authors declare no conflict of interest.

Data Availability Statement

The data that support the findings of this study are available in the Supporting Information of this article.

Keywords

chirality inversion, circular dichroism, circularly polarized luminescence, conformational homogeneity, crystal growth, peptoids, pyrenes

Received: October 4, 2023
Revised: November 13, 2023
Published online: December 1, 2023

[1] R. J. Simon, R. S. Kania, R. N. Zuckermann, V. D. Huebner, D. A. Jewell, S. Banville, S. Ng, L. Wang, S. Rosenberg, C. K. Marlowe, *Proc. Natl. Acad. Sci. U. S. A.* **1992**, *89*, 9367.
[2] P. Armand, K. Kirshenbaum, A. Falicov, R. L. Dunbrack, K. A. Dill, R. N. Zuckermann, F. E. Cohen, *Folding Des.* **1997**, *2*, 369.
[3] P. Armand, K. Kirshenbaum, R. A. Goldsmith, S. Farr-Jones, A. E. Barron, K. T. V. Truong, K. A. Dill, D. F. Mierke, F. E. Cohen, R. N. Zuckermann, E. K. Bradley, *Proc. Natl. Acad. Sci. U. S. A.* **1998**, *95*, 4309.
[4] K. Kirshenbaum, A. E. Barron, R. A. Goldsmith, P. Armand, E. K. Bradley, K. T. V. Truong, K. A. Dill, F. E. Cohen, R. N. Zuckermann, *Proc. Natl. Acad. Sci. U. S. A.* **1998**, *95*, 4303.
[5] C. W. Wu, T. J. Sanborn, K. Huang, R. N. Zuckermann, A. E. Barron, *J. Am. Chem. Soc.* **2001**, *123*, 6778.
[6] C. W. Wu, K. Kirshenbaum, T. J. Sanborn, J. A. Patch, K. Huang, K. A. Dill, R. N. Zuckermann, A. E. Barron, *J. Am. Chem. Soc.* **2003**, *125*, 13525.
[7] B. C. Gorske, B. L. Bastian, G. D. Geske, H. E. Blackwell, *J. Am. Chem. Soc.* **2007**, *129*, 8928.
[8] N. H. Shah, G. L. Butterfoss, K. Nguyen, B. Yoo, R. Bonneau, D. L. Rabenstein, K. Kirshenbaum, *J. Am. Chem. Soc.* **2008**, *130*, 16622.

[9] J. R. Stringer, J. A. Crapster, I. A. Guzei, H. E. Blackwell, *J. Am. Chem. Soc.* **2011**, *133*, 15559.
[10] O. Roy, G. Dumonteil, S. Faure, L. Jouffret, A. Kriznik, C. Taillefumier, *J. Am. Chem. Soc.* **2017**, *139*, 13533.
[11] K. Huang, C. W. Wu, T. J. Sanborn, J. A. Patch, K. Kirshenbaum, R. N. Zuckermann, A. E. Barron, I. Radhakrishnan, *J. Am. Chem. Soc.* **2006**, *128*, 1733.
[12] S. B. Y. Shin, B. Yoo, L. J. Todaro, K. Kirshenbaum, *J. Am. Chem. Soc.* **2007**, *129*, 3218.
[13] N. P. Chongsiriwatana, J. A. Patch, A. M. Czyzewski, M. T. Dohm, A. Ivankin, D. Gidalevitz, R. N. Zuckermann, A. E. Barron, *Proc. Natl. Acad. Sci. U. S. A.* **2008**, *105*, 2794.
[14] M. Baskin, G. Maayan, *Chem. Sci.* **2016**, *7*, 2809.
[15] A. D'Amato, L. Jiang, G. Della Sala, K. Kirshenbaum, C. Costabile, C. Furlan, E. Gianolio, I. Izzo, F. De Riccardis, *J. Org. Chem.* **2023**, *88*, 6588.
[16] G. Maayan, M. D. Ward, K. Kirshenbaum, *Proc. Natl. Acad. Sci. U. S. A.* **2009**, *106*, 13679.
[17] W. Yang, J. Jo, H. Oh, H. Lee, W. J. Chung, J. Seo, *J. Org. Chem.* **2020**, *85*, 1392.
[18] D. Kim, Y. J. Lee, D. H. Ahn, J. W. Song, J. Seo, H. Lee, *J. Phys. Chem. Lett.* **2020**, *11*, 4668.
[19] B. C. Gorske, J. R. Stringer, B. L. Bastian, S. A. Fowler, H. E. Blackwell, *J. Am. Chem. Soc.* **2009**, *131*, 16555.
[20] I. Wellhöfer, K. Frydenyang, S. Kotesova, A. M. Christiansen, J. S. Laursen, C. A. Olsen, *J. Org. Chem.* **2019**, *84*, 3762.
[21] A. A. Fuller, J. Huber, C. J. Jimenez, K. M. Dowell, S. Hough, A. Ortega, K. N. McComas, J. Kunkel, P. Asuri, *Biopolymers* **2019**, *110*, e23248.
[22] A. A. Fuller, B. A. Yurash, E. N. Schaumann, F. J. Seidl, *Org. Lett.* **2013**, *15*, 5118.
[23] C. Hao, L. Xu, M. Sun, H. Zhang, H. Kuang, C. Xu, *Chem. Eur. J.* **2019**, *25*, 12235.
[24] P. Stachelek, L. MacKenzie, D. Parker, R. Pal, *Nat. Commun.* **2022**, *13*, 553.
[25] L. Xu, Y. Feng, D. Yu, Z. Zheng, X. Chen, W. Hong, *Adv. Mater. Technol.* **2020**, *5*, 2000373.
[26] T. Kawasaki, M. Sato, S. Ishiguro, T. Saito, Y. Morishita, I. Sato, H. Nishino, Y. Inoue, K. Soai, *J. Am. Chem. Soc.* **2005**, *127*, 3274.
[27] C. He, G. Yang, Y. Kuai, S. Shan, L. Yang, J. Hu, D. Zhang, Q. Zhang, G. Zou, *Nat. Commun.* **2018**, *9*, 5117.
[28] M. Deng, N. F. M. Mukthar, N. D. Schley, G. Ung, *Angew. Chem., Int. Ed.* **2020**, *59*, 1228.
[29] C. Maeda, K. Nagahata, T. Shirakawa, T. Ema, *Angew. Chem., Int. Ed.* **2020**, *59*, 7813.
[30] M. X. Yu, C. P. Liu, Y. F. Zhao, S. C. Li, Y. L. Yu, J. Q. Lv, L. Chen, F. L. Jiang, M. C. Hong, *Angew. Chem., Int. Ed.* **2022**, *61*, e202201590.
[31] K. Takaishi, S. Murakami, F. Yoshinami, T. Ema, *Angew. Chem., Int. Ed.* **2022**, *61*, e202204609.
[32] H. Zhang, J. Han, X. Jin, P. Duan, *Angew. Chem., Int. Ed.* **2021**, *60*, 4575.
[33] Y. Zhang, H. Li, Z. Geng, W. H. Zheng, Y. Quan, Y. Cheng, *ACS Nano* **2022**, *16*, 3173.
[34] J. Seo, A. E. Barron, R. N. Zuckermann, *Org. Lett.* **2010**, *12*, 492.
[35] R. N. Zuckermann, J. M. Kerr, S. B. H. Kent, W. H. Moos, *J. Am. Chem. Soc.* **1992**, *114*, 10646.
[36] D. Shin, J. Seo, *Bull. Korean Chem. Soc.* **2021**, *42*, 376.
[37] E. De Santis, T. Hjelmagaard, C. Caumes, S. Faure, B. D. Alexander, S. J. Holder, G. Siligardi, C. Taillefumier, A. A. Edwards, *Org. Biomol. Chem.* **2012**, *10*, 1108.
[38] J. A. Hodges, R. T. Raines, *Org. Lett.* **2006**, *8*, 4695.
[39] Deposition numbers 2195705 (for peptoid 1), 2195906 (for peptoid 2), 2195707 (for peptoid 1′), 2195708 (for peptoid 2′), 2195709 (for peptoid 3′), and 2195710 (for peptoid 4′) contain the supplementary crystallographic data for this paper. These data are provided free of charge by the joint Cambridge Crystallographic Data Centre and Fachinformationszentrum Karlsruhe Access Structures service.
[40] H. M. Shin, C. M. Kang, M. H. Yoon, J. Seo, *Chem. Commun.* **2014**, *50*, 4465.
[41] R. Pariser, *J. Chem. Phys.* **1956**, *24*, 250.
[42] N. Harada, K. Nakanishi, *Circular Dichroic Spectroscopy: Exciton Coupling In Organic Stereochemistry*, University Science Books, New York, NY **1983**.
[43] N. Berova, L. D. Di Bari, G. Pescitelli, *Chem. Soc. Rev.* **2007**, *36*, 914.